AIP Journal of Applied Physics

Ultrahigh electromechanical response in (1−x)(Na0.5Bi0.5)TiO3-xBaTiO3 single-crystals via polarization extension

Wenwei Ge, Chengtao Luo, Qinhui Zhang, Chris P. Devreugd, Yang Ren, Jiefang Li, Haosu Luo, and D. Viehland

Citation: Journal of Applied Physics **111**, 093508 (2012); doi: 10.1063/1.4709619
View online: http://dx.doi.org/10.1063/1.4709619
View Table of Contents: http://scitation.aip.org/content/aip/journal/jap/111/9?ver=pdfcov
Published by the AIP Publishing

Ultrahigh electromechanical response in $(1-x)(Na_{0.5}Bi_{0.5})TiO_3$-$xBaTiO_3$ single-crystals via polarization extension

Wenwei Ge,[1,a)] Chengtao Luo,[1] Qinhui Zhang,[2] Chris P. Devreugd,[1] Yang Ren,[3] Jiefang Li,[1] Haosu Luo,[2] and D. Viehland[1]
[1]*Department of Materials Science and Engineering, Virginia Tech, Blacksburg, Virginia 24061, USA*
[2]*Shanghai Institute of Ceramics, Chinese Academy of Sciences, Shanghai 201800, China*
[3]*Advanced Photon Source, Argonne National Laboratory, Argonne, Illinois 60439, USA*

(Received 13 January 2012; accepted 28 March 2012; published online 2 May 2012)

The dielectric, ferroelectric, and electric field-induced strain response of [001]-and [101]-oriented $0.944Na_{0.5}Bi_{0.5}TiO_3$-$0.056BaTiO_3$ (0.944NBT-0.056BT) single crystals were investigated as a function of temperature and dc bias (E). An ultrahigh electromechanical response with large amplitude longitudinal piezoelectric coefficients as high as $d_{33} = 2500$ pm/V was found in $[001]_{PC}$ oriented 0.944NBT-0.056BT single crystals near a depolarization temperature of $T_d = 130\,^{\circ}C$. *In-situ* XRD revealed that the enhanced piezoelectric properties resulted from a polarization extension between a polar pseudocubic phase with a slight tetragonal (*P4bm*) distortion and a polar tetragonal one with a large tetragonal distortion of $c/a = 1.02$. Our findings indicate a potential approach to high performance lead-free piezoelectrics, via polarization extension. © *2012 American Institute of Physics*. [http://dx.doi.org/10.1063/1.4709619]

I. INTRODUCTION

Lead zirconium titanate (PZT) ceramics are widely used in transducer, actuator, and other electromechanical applications. Lead has recently been expelled from many commercial applications and materials owing to concerns regarding its toxicity. This concern has stimulated significant research efforts in the search for high-performance lead-free piezoelectrics.[1–7]

In the search for lead-free materials with properties comparable to those of PZT, most efforts have focused on solid solutions having PZT-like morphotropic phase boundary (MPB) between tetragonal (T) and rhombohedral (R) ferroelectric phases.[8] It has been shown that phase transitions near MPBs between R and T phases actually occur by structurally bridging intermediate monoclinic (M) phases.[9] The high electromechanical responses are then believed to relate to symmetry-allowed polarization rotations[10–13] during which the transverse dielectric susceptibility χ_{11} and shear piezoelectric coefficient d_{15} are enhanced as discussed by Damjanovic.[14–19] The large piezoelectric response along non-polar axes is, then, a consequence of the large χ_{11} and d_{15} values.[19,20] Phenomenological calculations have also shown that the piezoelectric response along polar axes can be enhanced due to polarization extension.[19–21]

Solid solutions of $(1-x)Na_{0.5}Bi_{0.5}TiO_3$-$xBaTiO_3$ (abbreviated as $(1-x)$NBT-xBT) are potentially important lead-free piezoelectric systems, as their piezoelectric properties are enhanced near $0.06 < x < 0.08$.[22,23] Structural investigations revealed that $(1-x)$NBT-xBT has a coexistence of rhombohedral (R, $\frac{\Delta P_3}{\Delta E_3}$) and tetragonal (T, *P4bm*) phases for $0.06 < x < 0.08$.[23] The T (*P4bm*) structure is distorted from cubic by in-phase rotations of the TiO_6 octahedra about the $[001]_{PC}$: according to the tilt system $a^0a^0c^+$ (Glazer notation[24]), combined with antiparallel displacement of the Na^{1+}/Bi^{3+} and Ti^{4+} cations along $[001]_{PC}$, where the subscript PC corresponds to the indexing of the directions on the pseudocubic cell setting. A view of the *P4bm* structure down the $[010]_{PC}$ showing the relative cation displacements are given in Fig. 6(a). The presence of $a^0a^0c^+$ octahedral tilts gives rise to M-type superstructure reflections[24] such as $1/2(310)_{PC}$. The Na^{1+}/Bi^{3+} and Ti^{4+} cations displace almost equally in opposite directions along $[001]_{PC}$, which results in the T (*P4bm*) phase being only weakly polar. The R (*R3c*) structure is characterized by $a^-a^-a^-$ (Glazer notation[24]) antiphase octahedral rotations about $[111]_{PC}$ combined with parallel displacement of the Na^{1+}/Bi^{3+} and Ti^{4+} cations along the $[111]_{PC}$ axis.[25] The presence of $a^-a^-a^-$ octahedral tilts gives rise to R-type superstructure reflections[24] such as $1/2(311)_{PC}$. With increasing temperature from 25 °C to 200 °C, M-type reflections gain intensity, whereas R-type reflections gradually disappear.[25]

More recently, it was found when $(1-x)$NBT-xBT are co-modified with $K_{0.5}Na_{0.5}NbO_3$ (or KNN) to form a $(1-x-y)$NBT-xBT-yKNN ternary system that the piezoelectric properties can be further enhanced by shifting the T (*P4bm*) phase to room temperature.[26] In this case, the maximum strain can reach values of $S_{max} = 0.45\%$ under applied fields of $E = 80$ kV/cm.[27] The value of S_{max}/E_{max} then reaches 560 pm/V, which is higher than that for PZT ceramics.[1] These large property changes arise due to a field-induced transformation between nonpolar (or weakly polar) and ferroelectric phases.[28] High-resolution neutron diffraction has shown that the initial nonpolar (or weakly polar) phase of 0.92NBT-0.06BT-0.02KNN has a T (*P4bm*) structure with a tetragonal distortion of only 0.0258%.[26] By monitor the M- and R-type superstructure reflection changes under E-field, it was shown that the T (*P4bm*) phase undergoes a reversible transformation to ferroelectric R (*R3c*) phase, giving rise to large induced strains.[26–28] These results indicate that

a)Electronic mail: wenweige@vt.edu.

(1-*x*-*y*)NBT-*x*BT-yKNN might be a solid solution whose piezoelectric properties are enhanced by a polarization extension mechanism.[21] However, in polycrystalline materials, only some grains are favorably oriented with respect to the E-field: thus, full advantage of polarization extension cannot be achieved and property enhancement may be limited with respect to its potential.[21]

In the present work, $(1-x)$NBT-*x*BT single crystals were grown by a top-seeded solution growth (TSSG) method. An ultrahigh electromechanical response with large amplitude longitudinal piezoelectric coefficients as high as $d_{33} = 2500$ pm/V in $[001]_{PC}$ oriented 0.944NBT-0.056BT single crystals near a depolarization temperature of $T_d = 130\,^{\circ}C$ was obtained. Structural investigations show that this enhancement is due to polarization extension between weakly polar T (*P4bm*) and strongly polar T phases under E applied along $\langle 001\rangle_{PC}$.

II. EXPERIMENTAL PROCEDURE

Single crystals of $(1-x)$NBT-*x*BT were grown by a TSSG method using high purity (better than 99.99%) Na_2CO_3, Bi_2O_3, TiO_2, and $BaCO_3$ as raw materials. These raw materials were mixed according to a stoichiometric ratio of $(Na_{0.5}Bi_{0.5})_{0.9}Ba_{0.1}TiO_3$, with a 20 wt. % excess of Na_2CO_3 and Bi_2O_3 as a self-flux. The mixed raw materials were put into a platinum crucible and heated to 1100 °C for 10 h to decompose the carbonates. Then $(1-x)$NBT-*x*BT single crystals were grown using a $\langle 001\rangle_{PC}$ oriented NBT crystal seed, which was heated by using a resistance furnace under an air atmosphere. The pulling rate was 1.2–1.5 mm/day and the rotating rate was 10 rpm. After growth, the crystals were removed from the flux-melt surface and cooled to room temperature at a rate of 30 °C/h.

The concentrations of Ba ions in the as-grown condition were determined by inductive coupled plasma atomic emission spectrometry (ICP-AES) to be 5.6 at. %. Pseudocubic $\langle 001\rangle_{PC}$ and $\langle 101\rangle_{PC}$ oriented 0.944NBT-0.056BT crystal wafers with dimensions of $2 \times 2 \times 0.4$ mm^3 were cut from the boule and subsequently electroded on both surfaces with gold. Temperature dependent dielectric constant measurements were performed using a LCR meter (HP 4284 A) under zero-field heating conditions in the temperature range of 30 to 600 °C. Polarization (P-E) and unipolar strain (ε-E) hysteresis loops were measured at a frequency of 1 Hz, using a modified Sawyer-Tower circuit and a linear variable differential transducer (LVDT) driven by a lock-in amplifier (Stanford Research, SR850) in the temperature range from 25 °C to 180 °C. Longitudinal piezoelectric d_{33} constants were measured using a quasistatic Berlincourt meter. E-Field dependent $(200)_{PC}$, $(220)_{PC}$, and $(222)_{PC}$ 2θ line scans and reciprocal-space (ω versus 2θ) maps were taken at various temperatures with increasing E-field between 0 and 20 kV/cm and then decreasing E-field from 20 to 0 kV/cm. These studies were done using a Philips MPD high-resolution x-ray diffraction system, equipped with a two bounce hybrid monochromator, an open three-circle Eulerian cradle, and a domed hot-stage. A Ge (220)-cut crystal was used as an analyzer, which had an angular resolution of 0.0068°. The x-ray wavelength was that of Cu$K_\alpha = 1.5406$ Å, and the x-ray generator was operated at 45 kV and 40 mA. During all the *in-situ* x-ray measurements, the E-field was applied along the $\langle 001\rangle_{PC}$ and $\langle 101\rangle_{PC}$ directions. The M-type superstructure reflections corresponding to the T (*P4bm*) structure of 0.944NBT-0.056BT were measured with $[001]_{PC}$ oriented crystals on the synchrotron radiation diffraction beam line 11-ID-C ($\lambda = 0.10798$ Å and E = 114.8 keV) at the Advanced Photon Sources (Argonne National Laboratory). The beam size was set to be 0.3×0.3 mm^2 by tungsten slits. The diffraction images were collected in the forward direction using a Perkin-Elmer large area detector.

III. RESULTS

A. Dielectric, ferroelectric, and piezoelectric properties

Figure 1(a) shows the dielectric constant ε_r and loss factor tan δ as a function of temperature for $\langle 001\rangle_{PC}$ oriented 0.944NBT-0.056BT, taken on heating. The results reveal a diffuse phase transformation with a broad dielectric maximum near $T_m = 285\,^{\circ}C$, near and just below which the dielectric constant was frequency independent. The so-called depolarization temperature (T_d) inherent to NBT (Ref. 29) was found to be decreased to $T_d = 145\,^{\circ}C$, below which notably frequency dispersion was found. The temperature T_d was frequency dependent and shifted to higher temperature with increasing frequency. Near T_d, a peak was found in the dielectric loss factor at 130 °C, below which tan δ was notably frequency dispersive. Please note that the dispersion in dielectric constant and loss factor was similar to that of relaxors below T_{max},[30] indicating polar heterogeneities with low frequency fluctuations.

Figure 1(b) shows polarization (P-E) hysteresis loops for $\langle 001\rangle_{PC}$ oriented 0.944NBT-0.056BT at various temperatures. At room temperature, the P-E loop saturated for $E \leq 50$ kV/cm, exhibiting a shape typical of ferroelectrics. The saturation polarization (P_s), remnant polarization (P_r) and coercive field (E_c) were 49.5 μC/cm^2, 46.4 μC/cm^2, and 28 kV/cm at room temperature. With increasing temperature between 25 °C and 100 °C, the values of P_s, P_r, and E_c were slightly decreased. On heating above 100 °C, P_s decreased slightly whereas P_r and E_c decreased sharply to 9.83 μC/cm^2 and 7 kV/cm. As a consequence, the hysteresis loop became "pinched" near 100 °C, which could indicate the coexistence of ferroelectric (FE) and nonpolar phases. With further increase of temperature towards T_d, the nonpolar phase became the dominant one, as can be seen from the double P-E loops at 130 °C and 150 °C where $P_r \approx 0$. These results in good agreement with previous reported P-E loops for 0.944NBT-0.056BT (Ref. 22) and 0.93NBT-0.06BT-0.01KNN (Ref. 28) ceramics. The temperature dependence of P_s and P_r is summarized in Fig. 1(c). The most notable change was a sharp drop in P_r: from about 39.3 μC/cm^2 at 80 °C to 9.83 μC/cm^2 at 100 °C, which then asymptotically converged to zero on heating to T_d, whereas, P_s slowly decreased from 49.5 μC/cm^2 to 24.9 μC/cm^2 with increasing temperature between 25 °C and 150 °C.

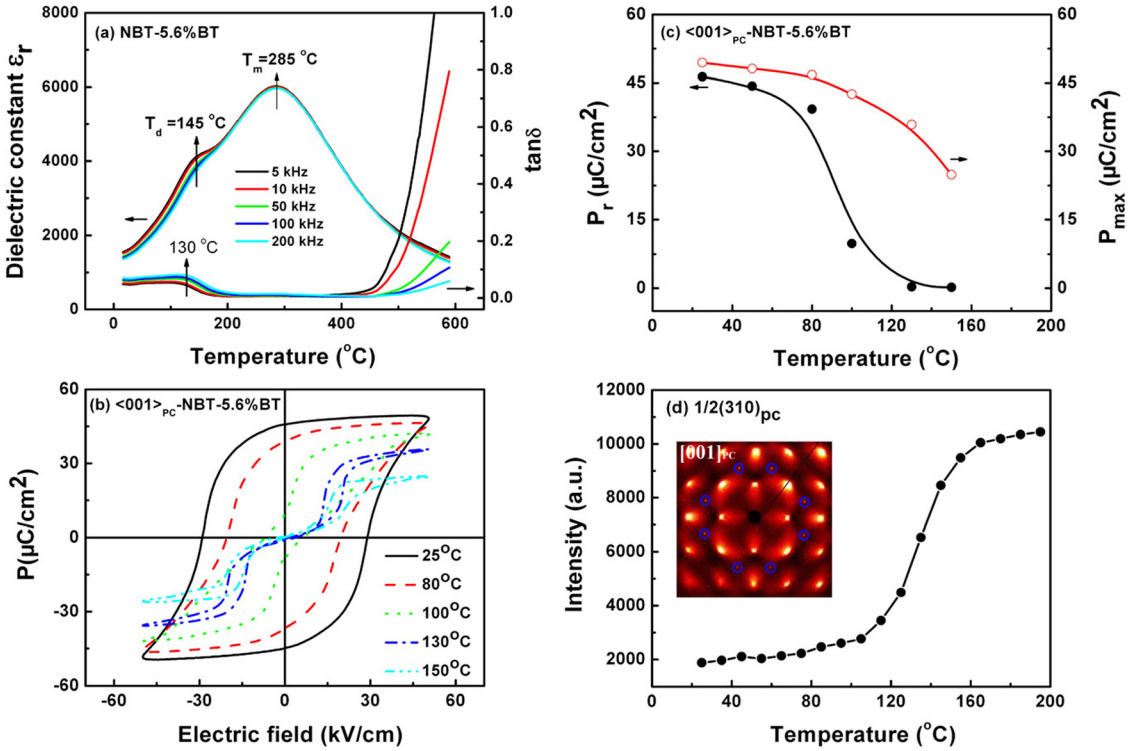

FIG. 1. (a) Temperature dependence of the dielectric constant ε_r and loss factor tan δ; (b) polarization (P-E) hysteresis loops at various temperatures; (c) temperature dependence of the remnant polarization (P_r) and induced maximum polarization (P_{max}) under $E_{max} = 50$ kV/cm; and (d) diffraction intensity of the $^1/_2(310)$ peak as a function of temperature for $\langle 001\rangle_{PC}$ oriented 0.944NBT-0.056BT crystal taken on heating. The inset in (d) show the x-ray scattering imaging pattern at 150°C. Circled spots indicate the presence of $^1/_2(310)$ super-lattice reflections corresponding with the $a^0a^0c^+$ (*P4bm*) octahedra tilting system.

The true nature of T_d is not yet fully understood.[29,31–33] Previously structural studies indicated that (1-*x*)NBT-*x*BT near the MPB does not have a notable deviation from cubic symmetry in the temperature range of 25 and 350 °C.[23,27,34–36] We conjecture that T_d is related to an $a^-a^-a^- \rightarrow a^0a^0c^+$ octahedral tilting transition. Figure 1(d) shows the temperature dependence of the $^1/_2(310)_{PC}$ super-lattice reflection in the temperature range between 25 °C and 200 °C. The inset of this figure shows a synchrotron x-ray scattering imaging pattern along $[001]_{PC}$ at 130 °C. The circled spots show the presence of $^1/_2(310)_{PC}$ super-lattice reflections, which indicate the existence of T (*P4bm*) structural regions having $a^0a^0c^+$ octahedral tilts. From Fig. 1(d), it can be seen that the intensities of these $^1/_2(310)_{PC}$ super-lattice reflections remained measurable at room temperature. This is consistent with previous transmission electron microscopy (TEM)[37,38] and neutron diffraction[36] studies which revealed the coexistence of dominant $a^-a^-a^-$-tilted (R3c) and small volume fractions of $a^0a^0c^+$-tilted (*P4bm*) structures for MPB $(1-x)$NBT-*x*BT. At room temperature, the dominant phase of 0.944NBT-0.056BT was *R3c*, with $P_r = 46.4\ \mu C/cm^2$. The volume fraction of the *R3c* phase was decreased with increasing temperature, whereas that of the weakly polar *P4bm* one increased. With increasing temperature between 100 °C and T_d, the intensity of the $^1/_2(310)_{PC}$ super-lattice reflection increased significantly (see Fig. 1(d)), indicating a transition from the polar *R3c* phase to a weakly polar *P4bm* one. This *R3c*→*P4bm* transition is consistent with changes in P_r which sharply decreased to zero at 130 °C (see Fig. 1(c)). Even though the *P4bm* phase is weakly polar at 130 °C, it could be fully saturated with $P_s = 35.9\ \mu C/cm^2$ under $E = 50$ kV/cm.

Figures 2(a) and 2(b) show ε-E curves for 0.944NBT-0.056BT measured along $\langle 001\rangle_{PC}$ and $\langle 101\rangle_{PC}$ at various temperatures under a maximum ac electric field of $E_{max} = 20$ kV/cm. Below 100 °C, the ε-E curves were nearly linear and anhysteretic. The maximum strains at 25 °C was $S_{max} = 0.08\%$ and 0.04% along $\langle 001\rangle_{PC}$ and $\langle 101\rangle_{PC}$, respectively. An approximation of the large signal value of d_{33} was derived from the slope of the ε-E curves: which were about 400 pm/V and 200 pm/V along $\langle 001\rangle_{PC}$ and $\langle 101\rangle_{PC}$, which are close to the values of 380 pC/N and 190 pC/N measured by a Berlincourt meter. At 100 °C, the value of S_{max} increased modestly to 0.17% and 0.06% along $\langle 001\rangle_{PC}$ and $\langle 101\rangle_{PC}$. On heating to 130 °C and 120 °C, the value of S_{max} increased significantly, reaching values of 0.60% and 0.20% along $\langle 001\rangle_{PC}$ and $\langle 101\rangle_{PC}$ under $E = 20$ kV/cm. With further increase of temperature, S_{max} decreased along both directions: in fact, no induced strain was apparent at 180 °C even for $E = 20$ kV/cm.

The temperature dependent ratio of S_{max}/E_{max} is shown in Figure 2(c). The value of S_{max}/E_{max} along $\langle 001\rangle_{PC}$ was higher than that along $\langle 101\rangle_{PC}$ in the temperature range of 25 °C to 170 °C. Below 110 °C, S_{max}/E_{max} along $\langle 101\rangle_{PC}$ varied in the range of 200–310 pm/V, whereas along $\langle 001\rangle_{PC}$, it ranged between 400 and 1000 pm/V. A sharp increase in S_{max}/E_{max} was observed along both directions near 120 °C to 130 °C: values as high as 3000 pm/V (130 °C) and 1000 pm/V (120 °C) were found along $\langle 001\rangle_{PC}$ and $\langle 101\rangle_{PC}$, respectively. These values are higher than those

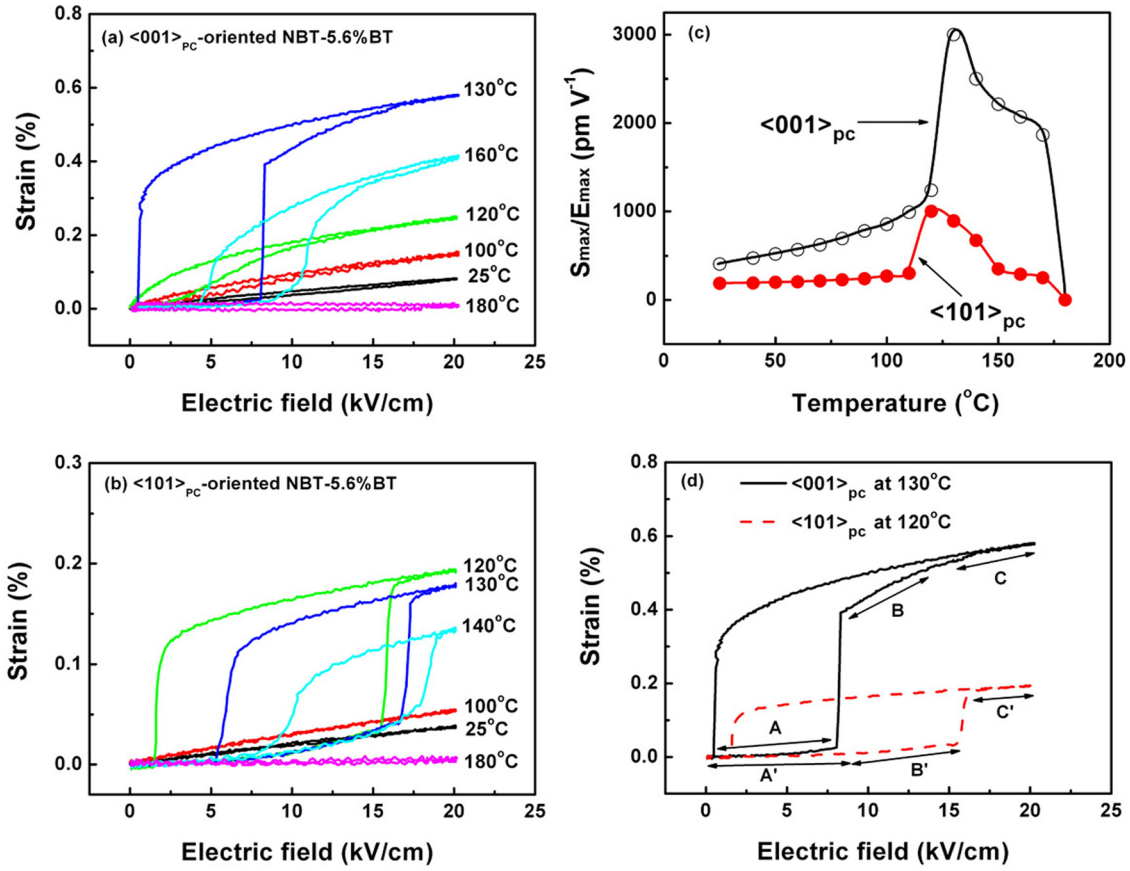

FIG. 2. Unipolar strain (ε-E) hysteresis loops of 0.944NBT-0.056BT measured along (a) $\langle 001\rangle_{PC}$ and (b) $\langle 101\rangle_{PC}$ at various temperatures; (c) S_{max}/E_{max} as determined form the unipolar strain curves; and (d) a comparison of the ε-E curves measured along $\langle 001\rangle_{PC}$ with that measured along $\langle 101\rangle_{PC}$ at 130°C and 120°C, respectively. The longitudinal piezoelectric coefficient d_{33} derived from the slope of steps A, B, C and A′, B′, and C′ are summarized in Table I.

previously reported for other Pb-free and Pb-containing piezo-ceramics and are comparable to those of Pb-containing relaxor-based single crystals.[1,27,39–45]

A comparison of the ε-E curves along $\langle 001\rangle_{PC}$ (solid line) and $\langle 101\rangle_{PC}$ (dashed line) (at 130 °C and 120 °C, respectively) is given in Figure 2(d). Three steps are identified in this figure that has notably different slops in the ε-E curves with increasing E along both directions. Large amplitude values for d_{33} derived from the ε-E slope for these steps are summarized in Table I. Along $\langle 001\rangle_{PC}$, the value of d_{33} was 350 pm/V, 2500 pm/V, and 720 pm/V for regions A (0–8 kV/cm), B (9–16 kV/cm), and C (16–20 kV/cm); whereas, along $\langle 101\rangle_{PC}$, the values were 75 pm/V, 485 pm/V, and 420 pm/V for regions A′ (0–9 kV/cm), B′ (10–15 kV/cm) and C′ (16–20 kV/cm). Clearly, there is the potential for giant d_{33} values in the vicinity of steps B and C: which might exceed that of conventional PZT ceramics[46] and which might be comparable to that of Pb-containing relaxor-based piezo-crystals.[44,45] However, the question must be asked: what is the mechanism of this large response?

B. Structural studies

To better understand the mechanism of this giant induced strain and large amplitude d_{33} value at 130 °C, *in-situ* high resolution x-ray diffraction (XRD) studies under E//$\langle 001\rangle_{PC}$ and E//$\langle 101\rangle_{PC}$ were performed for $0 \le E \le 20$ kV/cm. Figures 3(a)–3(c) show $(002)_{PC}$, $(202)_{PC}$, and $(111)_{PC}$ line scans taken at 130 °C for E//$\langle 001\rangle_{PC}$. The intensity is plotted on a sqrt scale, so that small peaks with low intensity can be more clearly seen. Under E = 0 kV/cm, only a single sharp 2θ peak was observed along the $(002)_{PC}$, $(202)_{PC}$, and $(111)_{PC}$ zones: which was also evident in ω-2θ area scans (see Figs. 5(a), 5(d), and 5(g)). The peak positions occurred $2\theta = 46.423°$, 67.769°, and 39.930° for $(002)_{PC}$, $(202)_{PC}$, and $(111)_{PC}$. The calculated d-spacing for these diffraction planes are consistent with a cubic structure having a lattice parameter of $a = 3.909 \pm 0.002$ Å. However, the $^1/_2(310)_{PC}$ super-lattice reflection in the synchrotron x-ray scattering imaging pattern at 130 °C (see inset of Fig. 1(d)) reveals that $a^0a^0c^+$ tilts exist in 0.944NBT-0.056BT, indicating slight tetragonal (*P4bm*) distortions which are too small to be detected within the resolution limit of our XRD system.

In Figure 3(a), it can be seen that the $(002)_{PC}$ peak was shifted slightly towards lower angles with increasing E between $0 \le E \le 8$ kV/cm. For E = 9 kV/cm, the $(002)_{PC}$ peak became much weaker and a new peak with a stronger intensity appeared at $2\theta = 46.065°$, indicating an E-field induced transformation. The E-field induced transformation was also reflected by changes in the $(202)_{PC}$ and $(111)_{PC}$ peak positions, as shown in Figures 3(b) and 3(c). Under 20 kV/cm, the dominant peaks were at $2\theta = 46.016°$, 67.568°, and 39.899° which were along the $(002)_{PC}$, $(202)_{PC}$,

TABLE I. Longitudinal piezoelectric coefficient d_{33} derived from the slope of steps A, B, and C of the ε-E curve along $\langle 001\rangle_{PC}$ (at 130°C) and A′, B′, and C′ of the ε-E curve along $\langle 101\rangle_{PC}$ (at 120°C) directions at 130°C (see Fig. 2(d)).

	d_{33} (pm/V) along $\langle 001\rangle_{pc}$	d_{33} (pm/V) along $\langle 101\rangle_{pc}$
Step A	350 (PC phase)	75 (PC phase)
Step B	2500 (PC+T)	485 (PC+T+R)
Step C	720 (T)	420 (T+R)

and $(111)_{PC}$ zones, respectively. The calculated d-spacing for the $(002)_{PC}$, $(202)_{PC}$, and $(111)_{PC}$ diffraction planes were consistent with a tetragonal structure having lattice parameters of $(a_t, c_t) = (3.895, 3.942)$Å. Figures 5(b), 5(e), and 5(h) show ω-2θ area scans at 130 °C under $E_{//[001]PC} = 20$ kV/cm taken about $(002)_{PC}$, $(202)_{PC}$, and $(111)_{PC}$, respectively. Only a single domain was observed in each of these scans, indicating the presence of a well-developed tetragonal c-domain state. The tetragonal distortion (c_t/a_t-1) was 0.012.

The evolution of the $(002)_{PC}$ peak profiles under E is shown in Figure 3(a). This data clearly reveal a transformation from a pseudo-cubic phase with a small tetragonal distortion to a T phase with a strong tetragonal distortion with increasing E//$[001]_{PC}$. For $0 < E < 8$ kV/cm, the peak position of 2θ value for $(001)_{PC}$ was slightly shifted towards lower angle, indicating a slight extension of the crystal lattice along $[001]_{PC}$. This is consistent with the induced strain for step A in the ε-E curve along $[001]_{PC}$ at 130 °C (see Figure 2(d)). With increasing E to 9 kV/cm, an intense $(002)_T$ peak became apparent, whereas the $(002)_{PC}$ became weaker. Clearly, a transformation to a T phase with a large c/a occurred. The intensity of $(002)_{PC}$ became increasingly weak for $E > 9$ kV/cm and was undetectable for $E \geq 16$ kV/cm. These results indicate that the pseudo-cubic and T phases coexist for $9\,\text{kV/cm} < E < 16\,\text{kV/cm}$ and that the volume fraction of the T phase is gradually increased. Above $E = 16$ kV/cm, the entire crystal is transformed to a single domain T state. The ultrahigh value of the large signal d_{33} value of step B in the ε-E curve (see Fig. 2(d)) may then be a consequence of this coexistence and reflected in an E-field induced change in the volume fraction, via length extension polarization mode. The large signal d_{33} value of 720 pm/V for $E \geq 16$ kV/cm for single c-domain state of step C (see Fig. 2(d)) is quite high, again indicating a polarization extension mode.

Figures 4(a)–4(c) show *in-situ* XRD line scans for $(202)_{PC}$, $(002)_{PC}$, and $(111)_{PC}$ reflections under E//$[101]_{PC}$ at 120 °C with increasing field for $0 \leq E \leq 20$ kV/cm. Under $E = 0$ kV/cm, only a single sharp peak was observed along each zone at 120 °C. The peak positions were determined to be $2\theta = 46.494°$, 67.853°, and 39.975°, respectively, and the lattice parameters of this pseudo-cubic structure were $a = 3.903 \pm 0.002$ Å. With increasing E in the range of 0 to 8 kV/cm, the 2θ position of $(202)_{PC}$ peak was slightly shifted

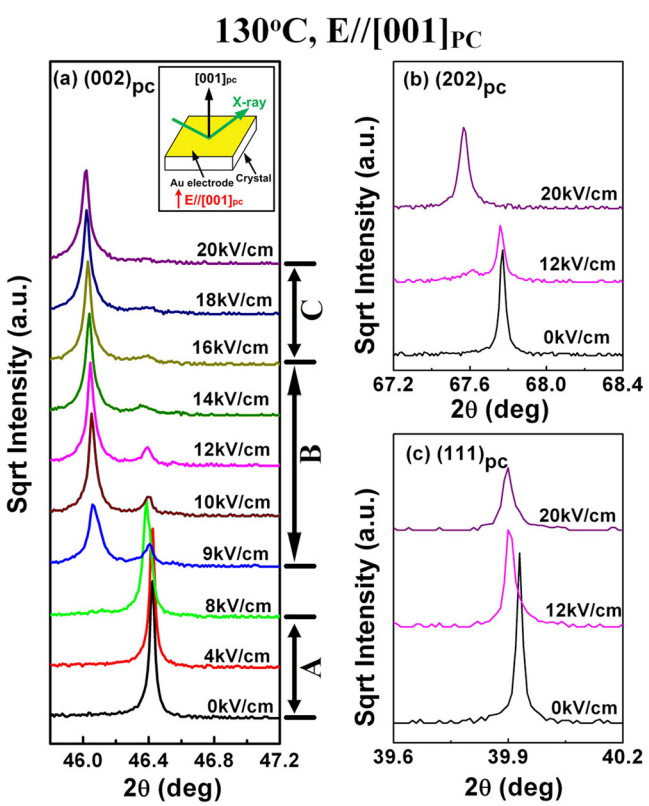

FIG. 3. *In-situ* x-ray line scans of (a) $(002)_{PC}$, (b) $(202)_{PC}$, and (c) $(111)_{PC}$ with increasing E-field under E//$[001]_{PC}$ for 0.944NBT-0.056BT crystals at 130°C. The E-field configuration during XRD measurements is shown in the inset of (a). Steps A, B, and C correspond to the steps on ε-E curves along $[001]_{PC}$ shown in Fig. 2(d).

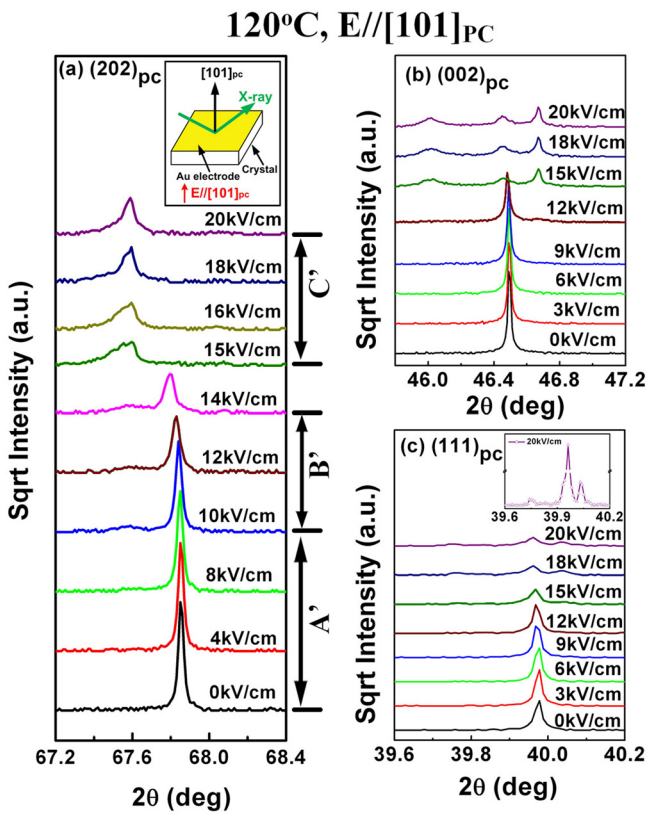

FIG. 4. *In-situ* x-ray line scans of (a) $(202)_{PC}$, (b) $(002)_{PC}$, and (c) $(111)_{PC}$ with increasing E-field under E//$[101]_{PC}$ for 0.944NBT-0.056BT crystals at 120°C. The E-field configuration during XRD measurements is shown in the inset of (a). Steps A′, B′, and C′ correspond to the steps on ε-E curves along $[101]_{PC}$ shown in Fig. 2(d).

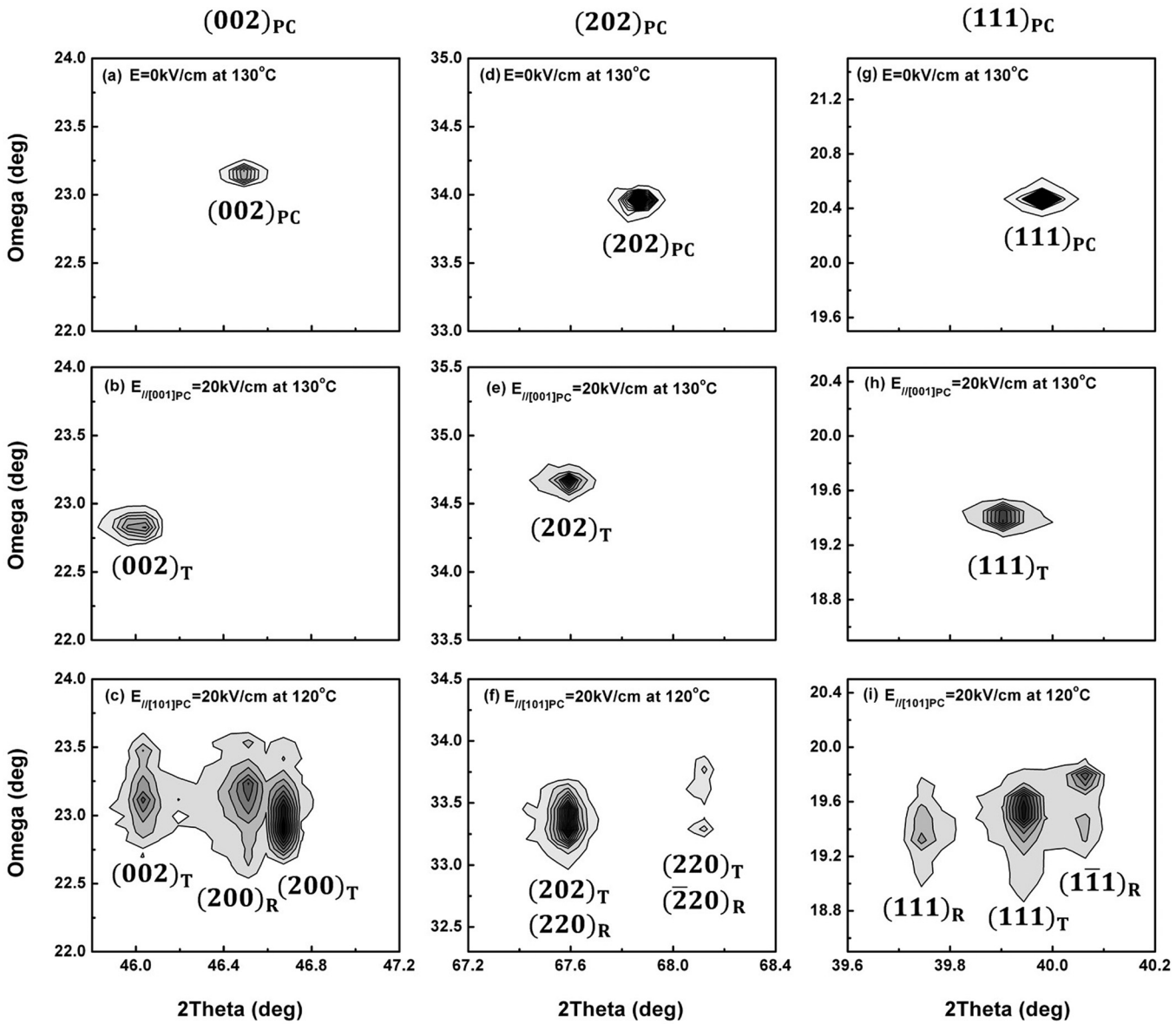

FIG. 5. ω-2θ maps for $(002)_{PC}$, $(202)_{PC}$, and $(111)_{PC}$ collected [(a), (d), and (g) at 130 °C] under E = 0 kV/cm, [(b), (e), and (h) at 130°C] under $E_{//[001]PC} = 20$ kV/cm, and [(c), (f), and (i) at 120°C] under $E_{//[101]PC} = 20$ kV/cm.

towards lower angle values. This shift became more pronounced at E = 10 kV/cm, and a 2nd weaker peak at $2\theta = 67.557°$ became noticeable. With further increasing E, the $(202)_{PC}$ peak continually shifted to lower 2θ values and became weaker. For E ≥ 15 kV/cm, the $(202)_{PC}$ peak at 67.853° was nearly undetectable, and only a single asymmetry peak at $2\theta = 67.557°$ was observable (see Fig. 4(a)). However, for E ≥ 15 kV/cm, the $(002)_{PC}$ peak exhibited a triplet splitting with peaks near $2\theta = 46.013°$, 46.453°, and 46.666° (see Fig. 4(b)). And, for E = 20 kV/cm, the $(111)_{PC}$ peak exhibited a triplet splitting with $2\theta = 39.739°$, 39.957°, and 40.026° (see Fig. 4(c)). The calculated d-spacing for $(002)_{PC}$, $(202)_{PC}$, and $(111)_{PC}$ diffraction plane under E = 20 kV/cm reveals a coexistence of T(a_t, c_t) = (3.890 ± 0.002, 3.942 ± 0.002)Å and R (a_r,α_r) = (3.907 ± 0.002 Å, 89.644°) phases.

Figures 5(c), 5(f), and 5(i) show ω-2θ area scans at 120 °C for $E_{//[101]PC} = 20$ kV/cm taken about $(002)_{PC}$, $(202)_{PC}$, and $(111)_{PC}$. Multi-domain states can be seen in each of these scans. For the ω-2θ area scan around $(002)_{PC}$, the three domain states with peaks at $2\theta = 46.013°$, 46.453°, and 46.666° correspond to $(002)_T$, $(200)_R$, and $(200)_T$ reflections. Along $(111)_{PC}$, area scans show three domain states at $2\theta = 39.739°$, 39.957°, and 40.026° that correspond to $(111)_R$, $(111)_T$, and $(1\bar{1}1)_R$ reflections. And, along $(202)_{PC}$, two domains were found at $2\theta = 67.557°$ and 68.122°, corresponding to $(202)_T$ overlapped with $(220)_R$ and to $(220)_T$ overlapped with $(\bar{2}20)_R$ reflections: the d-spacing of $(202)_T$ and $(220)_T$ is too close to those of $(220)_R$ and $(\bar{2}20)_R$ to be resolved. This overlap resulted in peak asymmetry ($2\theta = 67.557°$) in the linear scan for $E//_{[101]PC} \geq 15$ kV/cm (see Fig. 4(a)).

These results indicate two E-field induced phase transformation for $E//_{[101]PC} \geq 15$ kV/cm: (i) pseudo-cubic (slightly T distortion)→T (with strong T distortion) and (ii) pseudo-cubic → R. Accordingly, the three steps in the ε-E

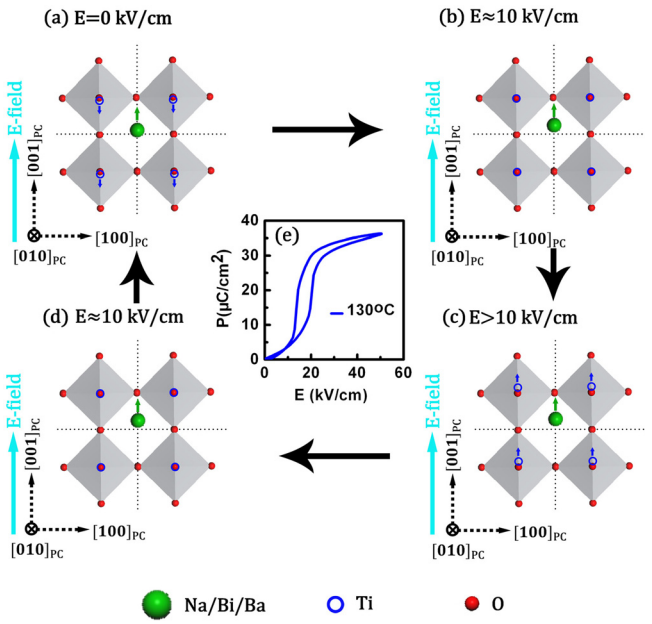

FIG. 6. Schematic illustrating the possible mechanism of polarization extension between weakly polar and strongly polar tetragonal phases, which is responsible for the ultrahigh electromechanical response in 0.944NBT-0.056BT single crystals along $[001]_{PC}$ at 130°C: (a) Projection of the weakly polar tetragonal (*P4bm*) structure along $[010]_{PC}$, showing the relative cation displacements. The large closed circles represent the Na/Bi sites, the small closed ones represent O sites, and the open circles represent Ti sites in the TiO_6 octahedra; (b) Ti^{4+} cations go back to the center along $[001]_{PC}$ direction under E ≈ 10 kV/cm; (c) E-field induced polar T phase with strong tetragonal distortion by moving Ti^{4+} cations away center along $[001]_{PC}$ under E > 10 kV/cm; and (d) Ti^{4+} cations go back to the center along $[00\bar{1}]_{PC}$ direction under E ≈ 10 kV/cm during subsequent E-field decreasing cycle. After E-field removal, the sample was brought back to the initial weak polar *P4bm* phase (a).

curves (see Fig. 2(d)) can be identified from the structural data to be (i) E < 10 kV/cm, stable pseudo-cubic or step A′ where $d_{33} = 75$ pm/V; (ii) 10 kV/cm ≤ E ≤ 14 kV/cm, E-field induced T and R phases coexisting with a pseudo-cubic one, or step B′ where $d_{33} = 485$ pm/V; and (iii) E ≥ 15 kV/cm, complete transformation into a mixture phase of T and R phases or step C′ where $d_{33} = 420$ pm/V. Interestingly, the E-field induced R and T phases were distinct and individually identifiable by XRD, with no evidence of low symmetry structurally bridging phases (i.e., monoclinic).[9] This is in sharp contrast to lead-based MPBs between polar phases, where enhanced piezoelectricity results from polarization rotation via M phase. Clearly, a mechanism of piezoelectric enhancement for MPB in $(1-x)$NBT-xBT crystals is different from that in Pb-based systems.

IV. DISCUSSION AND SUMMARY

Ab-initio and phenomenological calculations have both shown a flattening of the free energy profile near MPB regions.[10,13,16,17] It has also previously been pointed out that polarization rotation is not the only mechanism for property enhancement, but rather polarization extension contributions can also contribute.[19] The ultrahigh electromechanical response of 0.944NBT–0.056BT in step B (see Fig. 2(d)) can be explained by such a polarization extension, between weakly T and strongly T phases, as schematically illustrated in Figure 6. The initial structure near 130 °C is pseudocubic, with only weak T distortions (*P4bm*) where the $Na^{1+}/Bi^{3+}/Ba^{2+}$ and Ti^{4+} cations are near equally displaced in opposite directions along $[001]_{PC}$ (see Fig. 6(a)). With increasing E// $[001]_{PC}$, the Ti^{4+} cations are shifted to the center along $[001]_{PC}$ (see Fig. 6(b)), during which process the polarization is slightly increased (without hysteresis) for E < 10 kV/cm (see Fig. 6(e)). For E ≥ 10 kV/cm, the Ti^{4+} cations move off-center along $[001]_{PC}$ (see Fig. 6(c)), resulting in a significantly enhanced T distortion and an induced transformation. Polarization extension along $[001]_{PC}$ increases rapidly near this induced transition for 10 kV/cm < E < 16 kV/cm. For E > 16 kV/cm, the entire crystal transforms into a T phase single c-domain sate. After removal of E, the initial weakly polar phase is recovered (see Fig. 6(a)). The slim P-E loop in Fig. 6(e) indicates that the hysteresis between weakly polar and strongly polar T phases is small: i.e., polarization extension is reversible.

Following Landau-Devonshire theory, the value of d_{33} can be given as[47]

$$d_{33} = 2 \cdot Q_{33} \cdot \varepsilon_{33} \cdot P_3, \tag{1}$$

where Q_{33}, ε_{33}, and P_3 are the electrostriction coefficient, dielectric constant, and polarization. The standard definition of the dielectric constant is[47]

$$\varepsilon_{33} = 1 + \frac{4\pi \cdot \Delta P_3}{\Delta E_3} \approx \frac{4\pi \cdot \Delta P_3}{\Delta E_3}, \tag{2}$$

where E_3 is external electric field. Thus, d_{33} can be given as

$$d_{33} = 8\pi \cdot Q_{33} \cdot \frac{\Delta P_3}{\Delta E_3} \cdot P_3 \tag{3}$$

This equation shows that d_{33} is proportional to the polarization change $\frac{\Delta P_3}{\Delta E_3}$ multiplied by the total polarization P_3. For E < 10 kV/cm, both $\frac{\Delta P_3}{\Delta E_3}$ and P_3 of 0.944NBT-0.056BT are small, thus a relative small $d_{33} \sim 350$ pm/V was obtained for step A. With increasing E between 10 kV/cm and 16 kV/cm, both $\frac{\Delta P_3}{\Delta E_3}$ and P_3 sharply increased due to polarization extension, thus d_{33} increased significantly to values as high as 2500 pm/V. For E > 20 kV/cm, the polarization is saturated, and $\frac{\Delta P_3}{\Delta E_3}$ becomes smaller: thus, d_{33} is decreased for step C but remained relatively high at 700 pm/V.

For E//$[101]_{PC}$, coexisting T (strongly T distorted) and R phases were identified by XRD; however, no evidence of low symmetry structurally bridging M phases was found as for PMN-PT or PZN-PT.[9] This indicates that the polarization rotation between T and R phase does not occur near the MPB of (1-x)NBT-xBT. Rather, polarization extension form pseudo-cubic (slightly T distorted) → T (strongly T distorted) or R phases resulted in enhanced piezoelectricity. But the polarization extension direction is $[001]_{PC}$ for the T phase. Thus, the value of d_{33} along $[101]_{PC}$ is significantly smaller than that along $[001]_{PC}$. These results indicate that the enhancement of piezoelectric properties via polarization extension is strongly crystallographically dependent. In polycrystalline materials, only a few grains are favorably oriented with respect to E: thus, full advantage of polarization

extension can not be achieved and property enhancement limited with respect to its potential.[21] Thus, the possibility to get high performance lead-free piezoelectric, via polarization extension, lies within properly oriented single crystals.

In summary, an ultrahigh electromechanical response with longitudinal piezoelectric coefficients as high as $d_{33} = 2500$ pm/V was found in $[001]_{PC}$ oriented 0.944NBT-0.056BT single crystals near a depolarization temperature of $T_d = 130\,^{\circ}C$. *In-situ* XRD revealed that the enhanced piezoelectric properties resulted from a polarization extension between a polar pseudocubic phase with a slightly tetragonal (*P4bm*) distortion and a polar tetragonal phase with a large tetragonal distortion of $c/a = 1.02$. Our findings demonstrate a potential approach to high performance lead-free piezoelectrics in single crystals, via polarization extension.

ACKNOWLEDGMENTS

This work was supported by the National Science Foundation (Materials world network) DMR-0806592, by the Department of Energy under DE-FG02-07ER46480, by the Natural Science Foundation of China 50602047, by the Shanghai Municipal Government 08JC1420500, by the Innovation Fund of Shanghai Institute of Ceramics Y09ZC4140G, and by the Ministry of Science and Technology of China through 973 Program 2009CB623305.

[1]Y. Saito, H. Takao, T. Tani, T. Nonoyama, K. Takatori, T. Homma, T. Nagaya, and M. Nakamura, Nature **432**, 84 (2004).
[2]M. D. Maeder, D. Damjanovic, and N. Setter, J. Electroceram. **13**, 385 (2004).
[3]T. Takenaka and H. Nagata, J. Eur. Ceram. Soc. **25**, 2693 (2005).
[4]T. R. Shrout and S. J. Zhang, J. Electroceram. **19**, 111 (2007).
[5]P. K. Panda, J. Mater. Sci. **44**, 5049 (2009).
[6]J. Rodel, W. Jo, K. T. P. Seifert, E. M. Anton, T. Granzow, and D. Damjanovic, J. Am. Ceram. Soc. **92**, 1153 (2009).
[7]S. O. Leontsev and R. E. Eitel, Sci. Technol. Adv. Mater. **11**, 044302 (2010).
[8]B. Jaffe, J. Appl. Phys. **25**, 809 (1954).
[9]B. Noheda, D. E. Cox, G. Shirane, S. E. Park, L. E. Cross, and Z. Zhong, Phys. Rev. Lett. **86**, 3891 (2001).
[10]H. X. Fu and R. E. Cohen, Nature **403**, 281 (2000).
[11]R. E. Cohen, Nature **441**, 941 (2006).
[12]M. Ahart, M. Somayazulu, R. E. Cohen, P. Ganesh, P. Dera, H. K. Mao, R. J. Hemley, Y. Ren, P. Liermann, and Z. G. Wu, Nature **451**, 545 (2008).
[13]Z. G. Wu and R. E. Cohen, Phys. Rev. Lett. **95**, 037601 (2005).
[14]D. Damjanovic, F. Brem, and N. Setter, Appl. Phys. Lett. **80**, 652 (2002).
[15]M. Budimir, D. Damjanovic, and N. Setter, J. Appl. Phys. **94**, 6753 (2003).
[16]D. Damjanovic, J. Am. Ceram. Soc. **88**, 2663 (2005).
[17]M. Budimir, D. Damjanovic, and N. Setter, Phys. Rev. B **73**, 174106 (2006).
[18]D. Damjanovic, M. Budimir, M. Davis, and N. Setter, J. Mater. Sci. **41**, 65 (2006).
[19]D. Damjanovic, IEEE Trans. Ultrason. Ferroelectr. Freq. Control **56**, 1574 (2009).
[20]M. Davis, M. Budimir, D. Damjanovic, and N. Setter, J. Appl. Phys. **101**, 054112 (2007).
[21]D. Damjanovic, Appl. Phys. Lett. **97**, 062906 (2010).
[22]T. Takenaka, K. Maruyama, and K. Sakata, Jpn. J. Appl. Phys. **30**, 2236 (1991).
[23]W. Jo, J. E. Daniels, J. L. Jones, X. Tan, P. A. Thomas, D. Damjanovic, and J. Rödel, J. Appl. Phys. **109**, 014110 (2011).
[24]A. Glazer, Acta Crystallogr. **28**, 3384 (1972).
[25]G. O. Jones and P. A. Thomas, Acta Crystallogr., Sect. B: Struct. Sci. **58**, 168 (2002).
[26]M. Hinterstein, M. Knapp, M. Hölzel, W. Jo, A. Cervellino, H. Ehrenberg, and H. Fuess, J. Appl. Crystallogr. **43**, 1314 (2010).
[27]S. T. Zhang, A. B. Kounga, E. Aulbach, H. Ehrenberg, and J. Rodel, Appl. Phys. Lett. **91**, 112906 (2007).
[28]W. Jo, T. Granzow, E. Aulbach, J. Rodel, and D. Damjanovic, J. Appl. Phys. **105**, 094102 (2009).
[29]K. Sakata and Y. Masuda, Ferroelectrics **7**, 347 (1974).
[30]L. E. Cross, Ferroelectrics **151**, 305 (1994).
[31]J. Suchanicz, K. Roleder, A. Kania, and J. Hanaderek, Ferroelectrics **77**, 107 (1988).
[32]V. Isupov, Ferroelectrics **315**, 123 (2005).
[33]V. Dorcet, G. Trolliard, and P. Boullay, Chem. Mater. **20**, 5061 (2008).
[34]R. Ranjan and A. Dviwedi, Solid State Commun. **135**, 394 (2005).
[35]J. E. Daniels, W. Jo, J. Rodel, and J. L. Jones, Appl. Phys. Lett. **95**, 032904 (2009).
[36]H. Simons, J. Daniels, W. Jo, R. Dittmer, A. Studer, M. Avdeev, J. Rödel, and M. Hoffman, Appl. Phys. Lett. **98**, 082901 (2011).
[37]L. Schmitt, J. Kling, M. Hinterstein, M. Hoelzel, W. Jo, H. J. Kleebe, and H. Fuess, J. Mater. Sci. **46**, 4368 (2011).
[38]J. Kling, X. L. Tan, W. Jo, H. J. Kleebe, H. Fuess, and J. Rodel, J. Am. Ceram. Soc. **93**, 2452 (2010).
[39]E. Hollenstein, M. Davis, D. Damjanovic, and N. Setter, Appl. Phys. Lett. **87**, 182905 (2005).
[40]C. Ang, Z. Yu, Z. Jing, R. Guo, A. S. Bhalla, and L. E. Cross, Appl. Phys. Lett. **80**, 3424 (2002).
[41]S. J. Zhang, R. Xia, T. R. Shrout, G. Z. Zang, and J. F. Wang, J. Appl. Phys. **100**, 104108 (2006).
[42]E. M. Sabolsky, A. R. James, S. Kwon, S. Trolier-McKinstry, and G. L. Messing, Appl. Phys. Lett. **78**, 2551 (2001).
[43]E. M. Sabolsky, S. Trolier-McKinstry, and G. L. Messing, J. Appl. Phys. **93**, 4072 (2003).
[44]S. E. Park and T. R. Shrout, J. Appl. Phys. **82**, 1804 (1997).
[45]R. F. Service, Science **275**, 1878 (1997).
[46]B. Jaffe, W. R. Cook, and H. Jaffe, *Piezoelectric Ceramics* (Academic, London, 1971).
[47]R. E. Newnham, *Properties of Materials:Anisotropy, Symmetry, Structure* (Oxford University Press, Inc., New York, 2005).